Nanocrystalline α-Fe2O3: A Superparamagnetic Material for w-LED Application and Waste Water Treatment

Mahesh Gaidhane
Shri Lemdeo Patil Mahavidyalaya Mandhal
Deepak Taikar (deepak_taikar@yahoo.co.in)
Shri Lemdeo Patil Mahavidyalaya Mandhal https://orcid.org/0000-0001-8529-2214
Pravin Gaidhane
Govindrao Wanjari College of Engineering and Technology
Kalpana Nagde
Institute of Science Nagpur

Research Article

Keywords: Sol-gel, α-Fe2O3, Nanoparticles, Superparamagnetic, w-LED

Posted Date: March 23rd, 2021

DOI: https://doi.org/10.21203/rs.3.rs-327620/v1

Abstract

Nanocrystalline α-Fe_2O_3 is synthesized by sol-gel technique. The prepared nanomaterial was characterized by X-ray diffraction (XRD), SEM, TEM, Fourier Transform Infrared (FTIR) spectroscopy, Vibrating Sample Magnetometry (VSM) and photoluminescence (PL) techniques. X-ray powder diffraction analysis confirmed the formation of α-Fe_2O_3. Electron microscopy showed spherical morphologies with an average particle size of 30-40 nm. The magnetic property of the prepared material was studied by VSM at room temperature. VSM study shows superparamagnetic nature of the synthesized nanoparticles. Photoluminescence (PL) emission spectra show intense broad emission band centered at 570 nm with 393 nm excitation indicating its usefulness for w-LED application. The CIE-chromaticity color coordinates of prepared material were calculated. The photocatalytic activity of the α-Fe_2O_3 nanoparticles was analyzed and the nanopowder exhibited good photocatalytic activity for the removal AO7 from its aqueous solution.

1. Introduction

Among the various metal oxide nanoparticles, iron oxides nanoparticles have attracted the attention of modern researchers due to their wide range of technical applications. Iron oxides of different form (FeO, Fe_2O_3 and Fe_3O_4) in different phases (α-Fe_2O_3, β-Fe_2O_3, γ-Fe_2O_3 and ε-Fe_2O_3) have attracted a great deal of interest because of their numerous applications in different fields [1]. Among these, hematite (α-Fe_2O_3) is the most stable, low-cost, low-toxic, abundantly available, nature friendly semiconductor oxide [2]. Because of their catalytic, tunable magnetic and optical properties, α-Fe_2O_3 nanoparticles have attracted attention in the field of gas sensors, magnetic storage devices, catalytic reactions, paint manufacturing, lithium-iron batteries, ferro fluids, magnetic resonance imaging, biomedical applications, etc. [3–13].

Many synthesis methods have been used to prepare Fe_2O_3 nanoparticles [14–18]. A. Jahagirdar et al. [2] synthesized dumbbell shaped α-Fe_2O_3 nanoparticles by a low temperature combustion method and studied it's structural, magnetic and luminescence properties. Mitra and colleagues investigated the dependency of magnetic behavior of α-Fe_2O_3 to morphological aspects [19]. S. Jayanthi et al. [20] studied the diversity of magnetic properties such as saturation magnetization, coercivity and remenance of α-Fe_2O_3 nanoparticles at different temperatures. Recently, the impact of capping agents on structural, physico-chemical and biological properties of α-Fe_2O_3 has been investigated [21]. Tailoring of optical band gap and magnetic properties of α-Fe_2O_3 nanoparticles by pulse laser ablation in various aqueous media have been reported by Pandey et al. [22]. The controlled growth of α-Fe_2O_3 to show shape dependence magnetic properties was studied by Bharathi et al. [23]. T. Ohmori et al. [24] reported oxygen evolution on α-Fe_2O_3 by photocataylitic activity. The use of α-Fe_2O_3 as a photoanode for the photoassisted electrolysis of water was studied by J. H. Kennedy et al. [25]. Iron oxide has small band gap energy of 2 to 2.2 eV and can absorb light up to 600 nm. α-Fe_2O_3, has shown its usefulness for the removal of dyes from their aqueous solutions [26–28]. The Fe_2O_3 is a prominent catalyst for the photo-

squalor of unrefined pollutants. The Fe_2O_3 is widely available in nature and also mass-producible [29]. A. Rufus et al. reported the antibacterial activity of α-Fe_2O_3 [30]. In this paper, synthesis of α-Fe_2O_3 nanopowder using solgel method and its magnetic, photocatalytic, and PL properties were investigated and discussed.

2. Experimental

2.1 Materials and Method

The α-Fe_2O_3 nanoparticles were synthesized via sol-gel method by using citric acid. To synthesize α-Fe_2O_3 nanoparticles, iron(III) nitrate nonahydrate [$Fe(NO_3)_3.9H_2O$], citric acid and sodium hydroxide (NaOH) all are AR grade were used. Initially, 2 gm of $Fe(NO_3)_3.9H_2O$ was dissolved in 70 ml of double distilled water and stirred for 15 min. Thereafter 4 gm of citric acid solution was added slowly to the above solution, and the mixture was stirred for 1.5 h. To adjust the pH value, the NaOH solution was added to the above mixed solution. The mixture was stirred on magnetic stirrer until the homogeneous solution was obtained. The homogeneous solution was continued to stirred and heated simultaneously at 80°C to get highly viscous residual. Further it was dried at 100°C, so that a gel precursor was formed which was annealed at 400°C for 4 h to obtain α-Fe_2O_3 nanoparticles.

2.2 Characterization Techniques

The crystalline phases of the synthesized nanopowder was identified by X-ray diffraction (XRD) patterns recorded on a Philips PANalytical X'pert Pro diffractometer using CuKα (λ=1.54059 Å) radiation over the 2θ range of 10°—70°. The X-ray tube operated at 30 mA and 40 kV. The average particle size was calculated using Debye-Scherrer's equation.

$$D = \frac{0.9\,\lambda}{\beta\,\cos\theta}$$

Where λ = 1.540598 Å is the wavelength of the incident X-ray beam; θ is the Bragg's diffraction angle; β is Full width at half maxima (FWHM).

The Fourier-transform infrared (FTIR) spectrum of the prepared nanopowder was recorded by Nicolette IMPACT 400 D FTIR spectrometer, with the frequency ranging from 400 to 4000 cm^{-1}. Morphological study of synthesized nanopowder was carried out using scanning electron microscopy recorded on (JEOL microscope model JSM6510LV) scanning electron microscope. Transmission Electron Microscopy (TEM) image were taken from JEOL TEM 2010 electron microscope operating at an applied voltage of 200 kV. The magnetic property of the sample was investigated using a Vibrating Sample Magnetometer (VSM) at room temperature. The UV–VIS photoluminescence (PL) spectrum was recorded at room temperature on a Hitachi F-4000 florescence spectrophotometer. For PL measurement, the xenon lamp of 150W was used as an excitation source. The emission and excitation spectra were recorded using a spectral slit of 1.5

nm. The color chromaticity coordinates were obtained according to Commission International de l'Eclairage (CIE) using Radiant Imaging color calculator.

2.3 Photocatalytic activity

To study the photocatalytic activity of prepared nanopowder, a mercury vapour lamp was used as a source of UV-radiation. 50 cm^3 of the AO7 solution was taken in reaction vessel and appropriate amount of the prepared nanopowder was added into the AO7 solution. The mixture was stirred under UV-radiation for 45 minutes and then centrifuged at 3000 rpm. The UV-visible spectrum of the supernatant was recorded in the wavelength of 300 to 700 nm with the help of ELICO SL 159 spectrophotometer. The percentage dye removal was calculated using equation [31]

$$\% \text{ dye degradation} = \frac{(C_o - C_e)}{C_o} X\ 100$$

where C_o and C_e corresponds to the initial and final concentration of dye before and after photo-irradiation.

3. Results And Discussions

3.1 XRD

The XRD pattern of synthesized α-Fe_2O_3 is shown in Fig. 1. The sharp and single diffraction peaks of the XRD pattern confirm the formation of crystalline α-Fe_2O_3. The pattern is compared with the major lines in the ICDD data file 84-0311 and the excellent match is seen. It shows rhombohedral centered hexagonal structure in space group R-3c (group number 167). The pattern shows peaks at an angle 2θ (in degree) 24.334, 33.443, 35.882, 41.18, 49.863, 54.551, 58.172, 62.942 and 64.484 corresponds to the reflection from (012), (104), (110), (113), (024), (116), (018), (214) and (300) crystal planes respectively. The average particle size of synthesized material was calculated from the XRD pattern using Debye Sherrer's formula, and is found to be 48 nm.

3.2 Crystal structure

α-Fe_2O_3 is corundum (Al_2O_3) type rhombohedral centered hexagonal structure. Fe is coordinated with six oxygen atom in such a way that there are three shorter (1.90Å) and three longer (1.97Å) Fe-O bond lengths. It forms a mixture of corner, edge and face-sharing FeO_6 octahedra as shown in Fig. 2. At the same time the O is coordinated with four equivalent Fe atoms to form distorted edge and corner-sharing OFe_4 trigonal pyramids.

3.3 Fourier-transform infrared (FTIR) spectroscopy

FTIR spectrum for the prepared nanoparticles is shown in the Fig. 3. The FTIR spectroscopy determines the presence of functional groups adsorbed on the surface of the synthesized material. The two absorption peaks below 1000 cm^{-1} represent characteristic features of α-Fe_2O_3 and are assigned to metal oxygen stretching frequencies. The peak at low frequency 457 cm^{-1} is attributed to Fe–O deformation in the octahedral site whereas the peak at slightly higher frequency 538 cm^{-1} refers to Fe–O deformation in the octahedral and tetrahedral sites of hematite (α-Fe_2O_3) [32]. The peak at 3400 cm^{-1} is attributed to the stretching vibration of water, indicating the existence of a little water absorbed on the surface of the nanopowder.

3.4 SEM/TEM analysis

Fig. 4 shows the SEM micrograph of the nanopowder. The SEM micrograph indicated that the agglomerated particles are in the range of 30-40 nm with spherical morphologies. The size and shape of nanoparticles depends largely on the synthesis method. Fig. 5 shows the TEM image of prepared nanoparticle.

3.5 Magnetic hysteresis measurement

The magnetic property of α-Fe_2O_3 nanoparticles was characterized by VSM at room temperature in an applied magnetic field sweeping from −10,000 to 10,000 Oe. Fig. 6 shows the magnetic hysteresis loop of prepared nanomaterial which characterizes the dependence of magnetization on the applied magnetic field. The prepared α-Fe_2O_3 nanoparticles has a coersive magnetic field of about 83.43 Oe which is less than the value reported in previous literature [30,33]. The coersivity depends on size and shape anisotropy of the synthesized particles. The remanent magnetization (M_r) was detected at 2.511 emu/g. The staturation magnetization (Ms) 8.87 emu/g was observed at approximately 6000 Oe. The magnetic properties of materials depend on factors such as size, crystallinity, crystal defect and surface structure [34]. From the hysteresis loop, we can conclude that the prepared nanoparticles appear to be superparamagnetic.

3.6 Photoluminescence study and CIE chromaticity diagram

Usually α-Fe_2O_3 in its bulk form does not exhibit photoluminescence due to the local forbidden d-band transition [35]. On the other hand nanostructured α-Fe_2O_3 has been reported to exhibit photoluminescence due to delocalization and quantization of electronic states [36]. Fig. 7 shows PL excitation emission spectra of synthesized α-Fe_2O_3 nanoparticles. The emission spectra monitored at 390 nm excitation exhibit broad band emission ranging from 450 to 670 nm centered at 570 nm attributed to near band edge emission. The excitation spectra monitored at 570 nm emission shows broad excitation band ranging from 250 to 470 nm with intensity maxima occur at 393 nm and shoulder around 325 nm. The excitation peak around 325 nm assigned to ligand to metal charge transfer (LMCT) transition whereas main excitation peak at 393 nm attributed to ligand field transitions [21]. As the PL excitation curve of the

synthesized material shows a good cover over the n-UV region, the synthesized nanomaterial is an attractive option for n-UV LED converted phosphor in w-LEDs (solid state lighting) application.

Fig. 8 shows CIE chromaticity diagram of synthesized α-Fe_2O_3 nanoparticles. The emission spectrum was converted to the CIE1931 chromaticity parameters using the PL data and interactive CIE software (CIE coordinate calculator). The colour coordinates for prepared α-Fe_2O_3 was found to be (0.439, 0.525) which is in yellow region.

3.7 Photocatalytic activity of the nanopowder

Acid Orange (*AO7*) is a common anionic azo dye having formula $C_{16}H_{11}N_2NaSO_4$ and molecular mass equal to 350.3243 g/mol. It is widely used in paper, cosmetic, leather, textile and agricultural industries [37]. Chemically, AO7 is 4-[(2- hydroxy-1-naphthyl)azo] benzene sulfonate. Like many other azo dyes, AO7 often dumped in industrial wastewater and possess health threats to humans as well as other living organisms [38]. It is highly toxic to the environment. Ingestion of AO7 can cause number of health issues such as irritation of the mucous membrane, eye, skin, and upper respiratory tract; nausea, severe headaches; dizziness; cyanosis of lip and nose; and loss of bone marrow leading to anemia [39]. It is also carcinogenic in nature and can lead to tumors as well [40-43]. The structure and absorption spectrum of AO7 are shown in Fig. 9 and 10 respectively. The maximum absorbance was observed at 485 nm.

The photocatalytic study was conducted by varying the dosage of the nanopowder from 0.2 to 2.5 g/L of the dye solution. The study was carried out for four 10, 15, 20, and 25 ppm concentrations of the dye solutions. The optimum dosage was determined by plotting the graph of C_e/C_o versus the dosage of the nanopowder. The optimum irradiation time was recorded from the plot of C_e/C_o versus the irradiation time.

Fig. 11 shows the effect of dosage of prepared α-Fe_2O_3 nanopowder on the rate of photocatalytic removal of AO7. Form figure it was observed that the percentage of dye removal increases with the increase in the amount of α-Fe_2O_3 nanopowder in AO7 solution. The observed result is due to the increase in number of active sites available for adsorption of the dye molecules on its surface [37]. The optimum dosage of prepared nonopowder was found to be 1 g/L for 10 and 15 ppm dye solutions, for 20 ppm dye solutions the optimum dosage was found to 1.2 g/L and on the other hand for 25 ppm dye solutions the optimum dosage of prepared nonopowder was found to 1.4 g/L. Beyond this optimum value the percentage dye removal was found to be insignificant. It is predicted that at higher concentration, the penetration of UV radiation into dye solution decreases and the scattering effect for UV radiation increases. Fig. 12 shows the effect of irradiation time on the rate of photocatalytic activity. The best irradiation time was found to be 40 minutes for 10, 15, and 20 ppm dye concentration whereas for 25 ppm concentration of dye solution the optimum irradiation time found to be 50 min. Beyond this irradiation time the percentage dye removal was found to be negligible. Photocatalytic study of the α-Fe_2O_3 nanoparticles shows that the prepared nanopowder is an attractive candidate for the removal AO7 from its aqueous solution.

4. Conclusion

Nanocrystalline α-Fe_2O_3 has been successfully synthesized by sol-gel method. The XRD pattern of synthesized α-Fe_2O_3 matches well with the ICDD file. The electron microscopy showed spherical morphologies with an average particle size of 30-40 nm, which is consistent with the average particle size calculated from Debye Sherrer's formula. VSM study at room temperature exhibit hysteresis loop, with coersive magnetic field = 83.43 Oe, M_r = 2.511 emu/g and Ms = 8.87 emu/g at around 6000 Oe indicating superparamagnetic nature of the synthesized nanoparticles. The photoluminescence excitation/emission spectra of synthesized nanocrystalline α-Fe_2O_3 shows broad band emission centered at 570 nm corresponds to near band edge emission. The excitation spectra shows broad excitation band cover UV, near UV and visible blue region attributed to ligand to metal charge transfer (LMCT) transition and ligand field transitions. Since the prepared nanomaterial is excitable in n-UV region it can be useful in n-UV excited w-LED application. From photocatalytic activity of the α-Fe_2O_3 nanoparticles we conclude that the prepared nanomaterial would have a potential application in dye wastewater treatment.

Declarations

Funding- The author(s) received no financial support for the research, authorship, and/or publication of this article.

Conflicts of interest/Competing interests- The authors declare that there are no known conflicts of interest associated with this publication that could have influenced its outcome.

Availability of data and material- The manuscript contains original results and are not published in other journals.

Code availability- Not Applicable

CRedit authorship contribution statement-

Writing - original draft preparation, Formal analysis and investigation: [**Deepak Taikar**]; Conceptualization and Methodology: [**Mahesh Gaidhane, Pravin Gaidhane**];

References

[1] W. Xinghong, L. Zhang, N. Yonghong, H. Jianming, C. Xiaofeng, J. Phys. Chem. C 113(17), 7003 (2009)

[2] A. A. Jahagirdar, N. Dhananjaya, D. L. Monika, C. R. Kesavulu, H. Nagabhushana, S. C. Sharma, B. M. Nagabhushana, C. Shivakumara, J. L. Rao, R. P. S. Chakradhar, Spectrochimica Acta Part A: Molecular and Biomolecular Spectroscopy 104, 512–518 (2013)

[3] K. Sivula, F. Le Formal, M. Grotzel, Chem. Sus. Chem. 4, 432-449 (2011)

[4] S. Piramana, S. Sundar, R. Mariappana, Y. Y. Kima, K. Min, Sens. Actuators, B 234, 386–394 (2016)

[5] X. Zhang, Q. Li, Mater. Lett. 62, 988–990 (2008)

[6] Z. H. Jing, S. H. Wu, Mater. Chem. Phys. 92, 600–603 (2005)

[7] S. Cabanas-Polo, M. Distaso, W. Peukert, A. R. Boccaccini, J. Nanosci. Nanotechnol. 15, 10149-10155 (2015)

[8] V. Kesavan, Sivanand, P.S.S. Chandrasekaran, Yu. Koltypin, A. Gedanken, (Angew. Chem. Int. Ed. 38, 1999), pp. 3521–3523

[9] L. H. Huo, W. Li, L. H. Lu, H. N. Cui, S. Q. Xi, J. Wang, B. Zhao, Y. C. Shen, Z. H. Lu, Chem. Mater. 12, 790–794 (2000)

[10] K. Suresh, K. C. Patil, J. Mater. Sci. Lett. 12, 572–574 (1993)

[11] M. Kroell, M. Pridoehl, G. Zimmermann, L. Pop, S. Odenbach, A. Hartwig, J. Magn. Magn. Mater. 289, 21–24 (2005)

[12] Y. S. Kang, S. Risbud, J. F. Rabolt, P. Stroeve, Chem. Mater. 8, 2209–2211 (1996)

[13] S. Zhang, X. J. Chen, C. R. Gu, Y. Zhang, J. D. Xu, Z. P. Bian, D. Yang, N. Gu, Nanoscale Res. Lett. 4, 70–77 (2009)

[14] M. Liu, Y. Fu, M. Xiao, J. Huang, J. Solid State Chem. 178, 2798 (2005)

[15] S. Giri, S. Samanta, S. Maji, S. Ganguli, A. Bhaumik, J. Magn. Magn. Mater. 285, 296 (2005)

[16] H. Wang, Wang-Chang Geng, Res. Chem. Intermed. 37, 523 (2011)

[17] P. Raming, A. Winnubst, C. Van Kats, P. Philipse, Journal of Colloid and Interface Science 249, 346 (2002)

[18] Y. S. Koo, B. K. Yun, J. Jung, J. Magn. 15(1), 21 (2010)

[19] S. Mitra, S. Das, K. Mandal, S. Chaudhuri, Nanotechnology 18, 275608–16 (2007)

[20] S. Amala Jayanthi , D. Muthu Gnana Theresa Nathan, J. Jayashainy, P. Sagayaraj, Mater. Chem. Phys. 162, 316-325 (2015)

[21] P. Sharma, S. Kumari, D. Ghosh, V. Yadav, A. Vij, P. Rawat, S. Kumar, C. Sinha, S. Saini, V. Sharma, Md Imtaiyaz Hassan, C. Srivastava, S. Majumder, Mater. Chem. Phys. 258, 123899 (2021)

[22] B. K. Pandey, A. K. Shahi, J. Shah, R. K. Kotnala, R. Gopal, Surf. Sci., 289, 462–471 (2014)

[23] S. Bharathi, D. Nataraj, M. Seetha, D. Mangalaraj, N. Ponpandian, Y. Masuda, K. Senthil, K. Yong, CrystEngComm. 12, 373–82 (2010)

[24] T. Ohmori, H. Takahashi, H. Mametsuka, E. Suzuki, Phys. Chem. Chem. Phys. 2, 3519-3522 (2000)

[25] J. H. Kennedy and M. Anderman, J. Electrochem. Soc. 130, 848 (1983)

[26] Y. S. Hu, A. Kleiman-Shwarsctein, A. Forman, D. Hazen, J. Park, E. McFarland, Chem. Mater. 20, 3805 (2008)

[27] I. Cesar, A. Kay, J. Martinez, M. Gratzel, J. Am. Chem. Soc. 128, 4582 (2006)

[28] R. Khurram, Z. Wang, Muhammad Fahad Ehsan, S. Peng, Maryam Shafiq, Bushra Khan RSC Adv. 10, 44997 (2020)

[29] X. Zhang , Y. G. Niu , X. D. Meng , Y. Li, J. P. Zhao, Cryst Eng Comm. 15, 8166–8172 (2013)

[30] A. Rufus, S. N. and D. Philip, RSC Adv. 6(96), 94206-94217 (2016)

[31] L. Karimi, S. Zohoori, Mohammad Esmail Yazdanshenas, J. Saudi Chem. Soc. 18, 581 (2014)

[32] G. Wu, X. Tan, G. Li, C. Hu, J. Alloys Compd. 504, 371–376(2010)

[33] M. Tadic, N. Citakovic, M. Panjan, B.Stanojevic, D. Markovic, D. Jovanovic, V. Spasojevi, J. Alloy. Compd. 543, 118-124 (2012)

[34] X. L. Xie, H. Q. Yang, F. H. Zhang, L. Li, J. H. Ma, H. Jiao, J. Y. Zhang, J. Alloys Compd. 477, 90–99 (2009)

[35] N. Tsuda, K. Nasu, A. Yanase and K. Siratori, Electronic Conduction in Oxide, ed. M. Cardona, Springer Series in Solid State Science 94, (Springer-Verlag, Berlin, 1991).

[36] P. Shikha, B.S. Randhawa, T.S. Kang, RSC Adv. 5, 51158–51168 (2015)

[37] Kun Guan, Peijiang Zhou, Junye Zhang, Longlong Zhu, Mater. Res. Express 7, 016529 (2020) https://doi.org/10.1088/2053-1591/ab6253

[38] I. Banat, P. Nigam, D. Singh, R. Marchant, Technol 58, 217-227 (1996)

[39] M. A. Brown, S. C. De Vito, Crit Review Environ Sci Technol 23, 249-324 (1993)

[40] V. Gupta, A. Mittal, V. Gajbe, J. Mittal, Ind Eng Chem Res 45, 1446-1453 (2006)

[41] Y. He, P. Bishop, J Environ Eng 120, 108-121 (1994)

[42] H. Perera, Int J Waste Resour 9, 367 (2019)

[43] V. K. Gupta, A. Mittal, V. Gajbe, J. Mittal, Industrial and Engineering Chemistry Research 45(4), 1446 (2006)

Figures

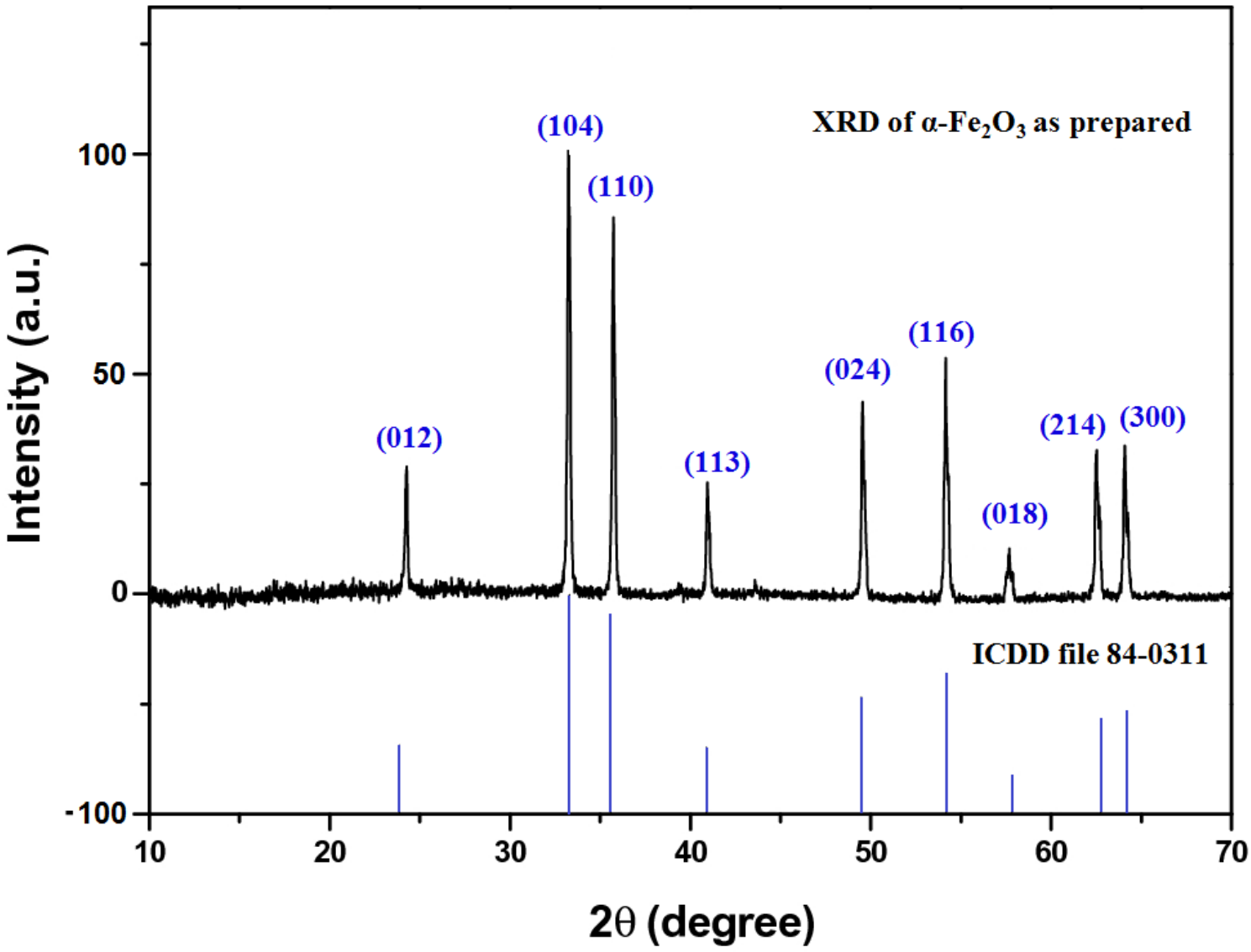

Figure 1

XRD results for α-Fe2O3 Diffraction pattern of α-Fe2O3 are compared with the stick pattern of ICDD file 84-0311

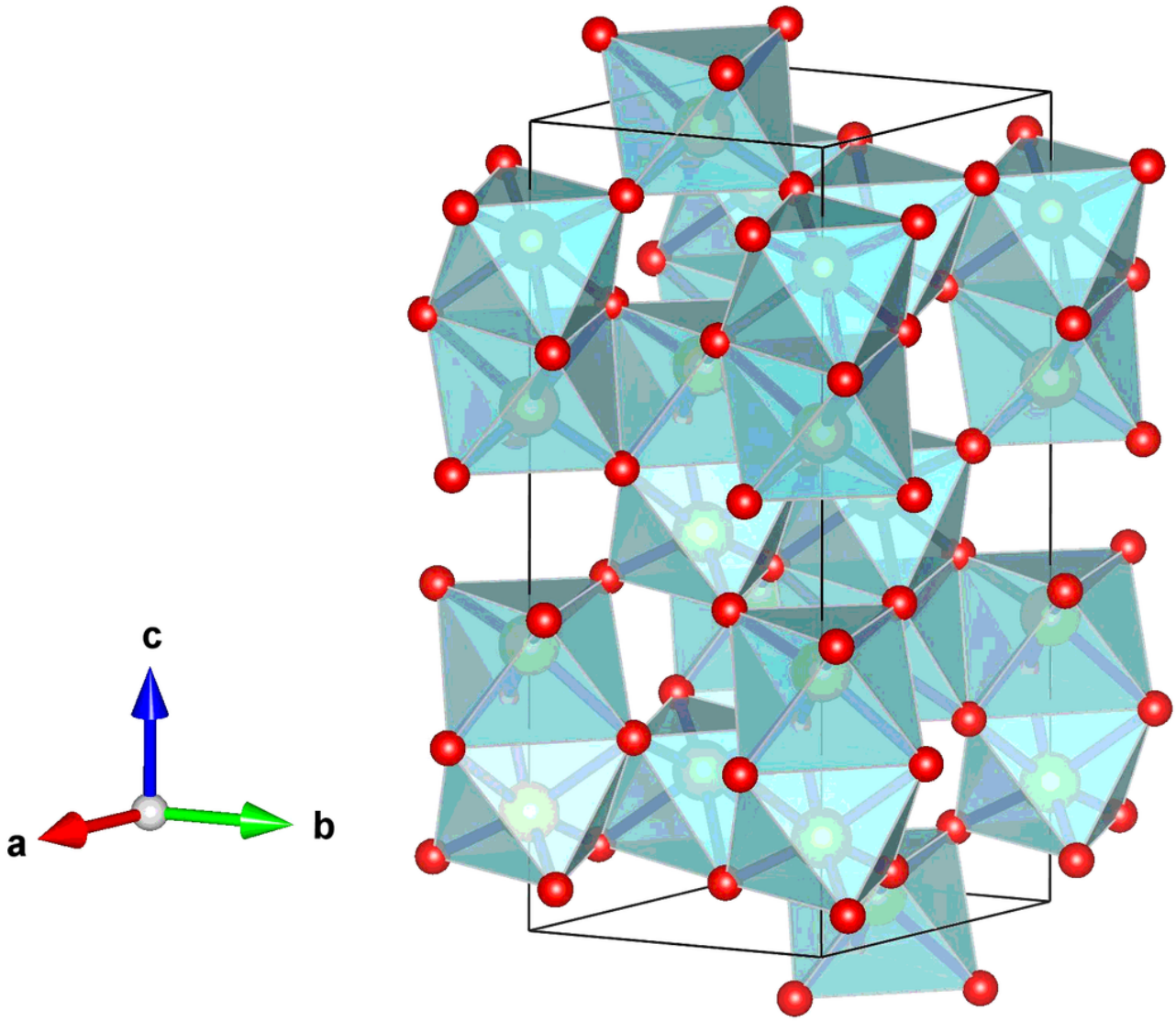

Figure 2

Crystal structure of α-Fe2O3

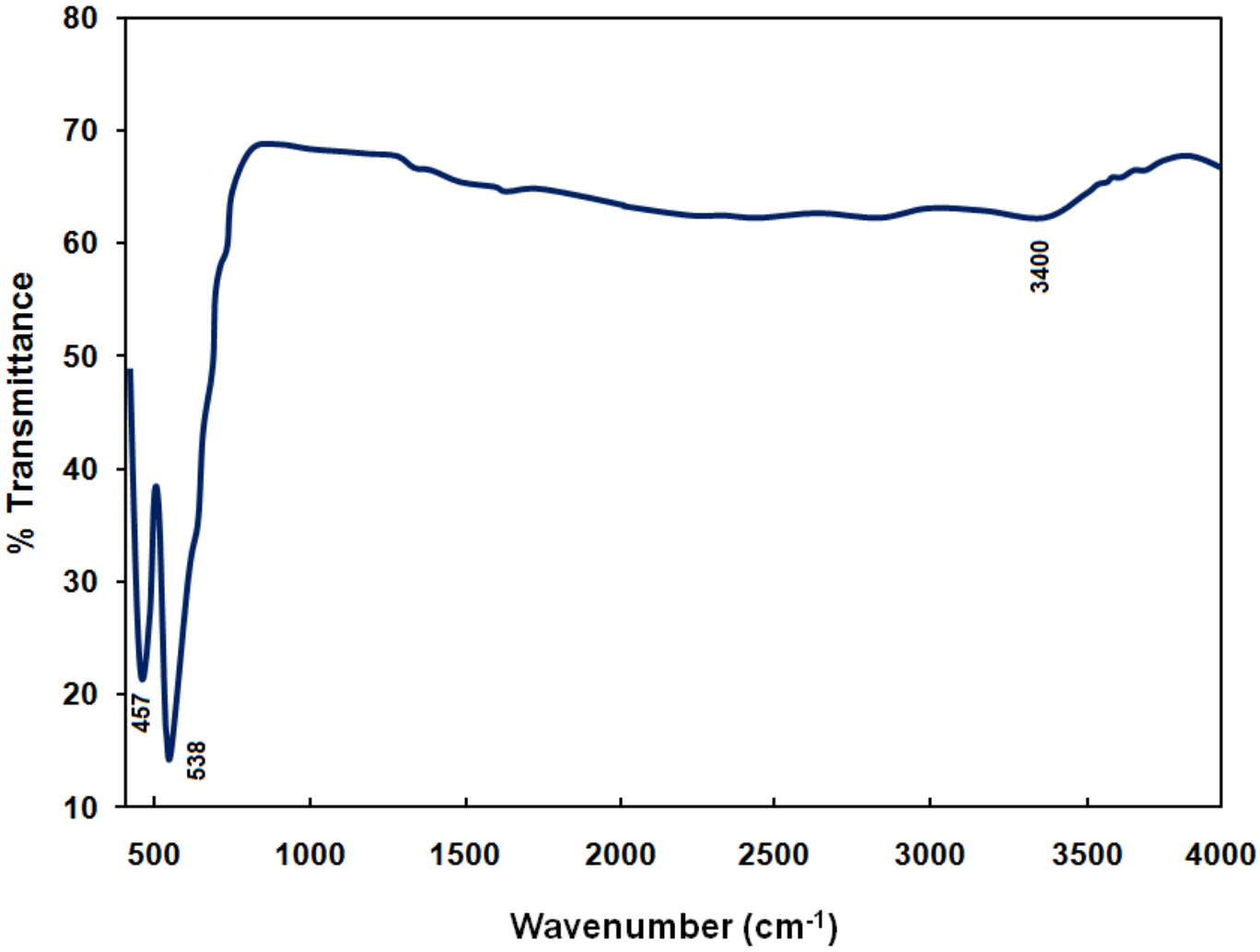

Figure 3

FTIR spectrum of prepared α-Fe2O3

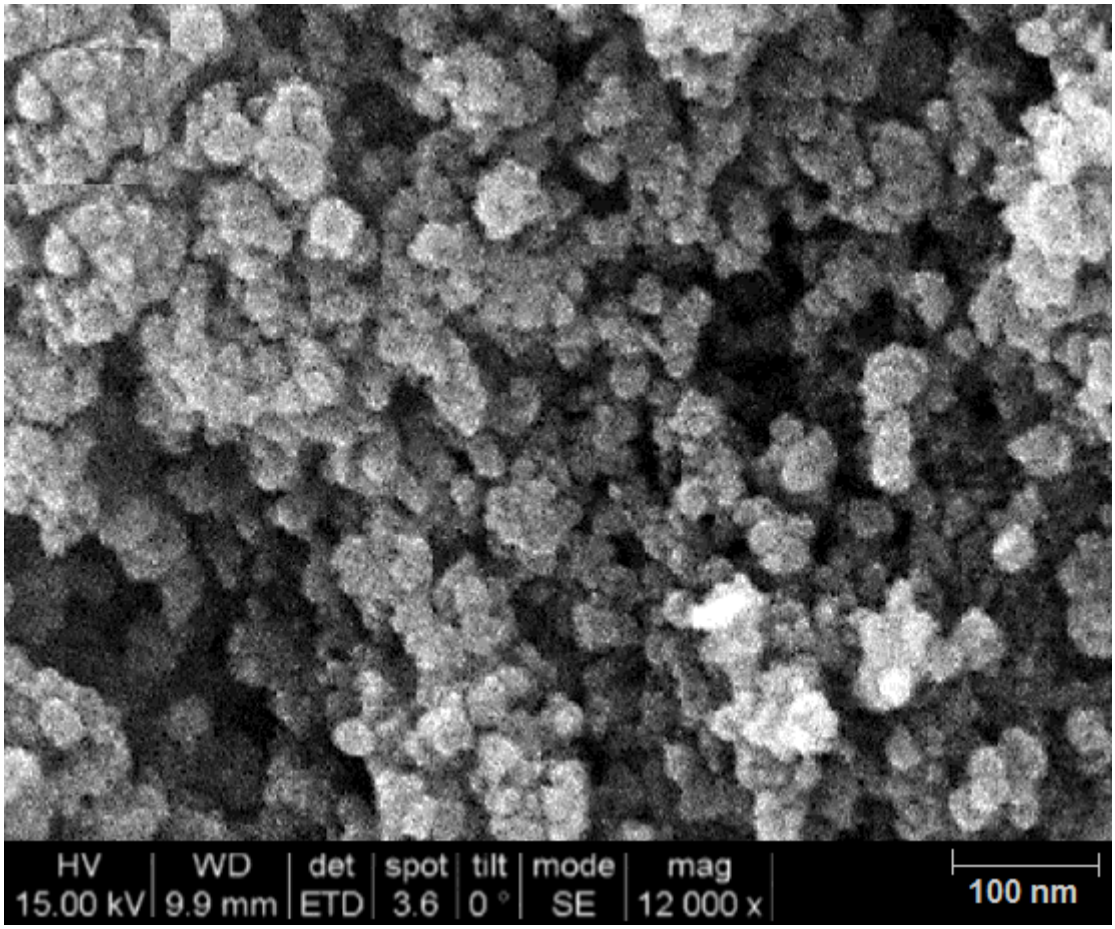

Figure 4

SEM micrographs of prepared α-Fe2O3

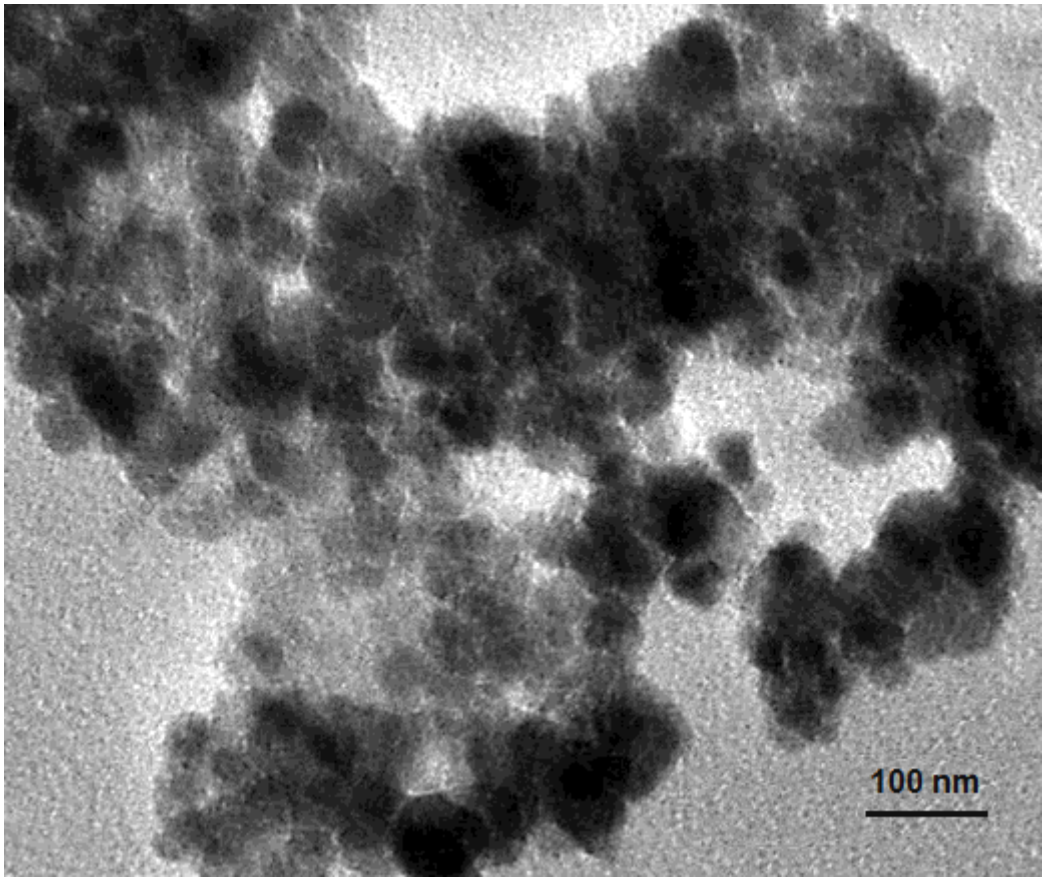

Figure 5

TEM image of prepared α-Fe2O3

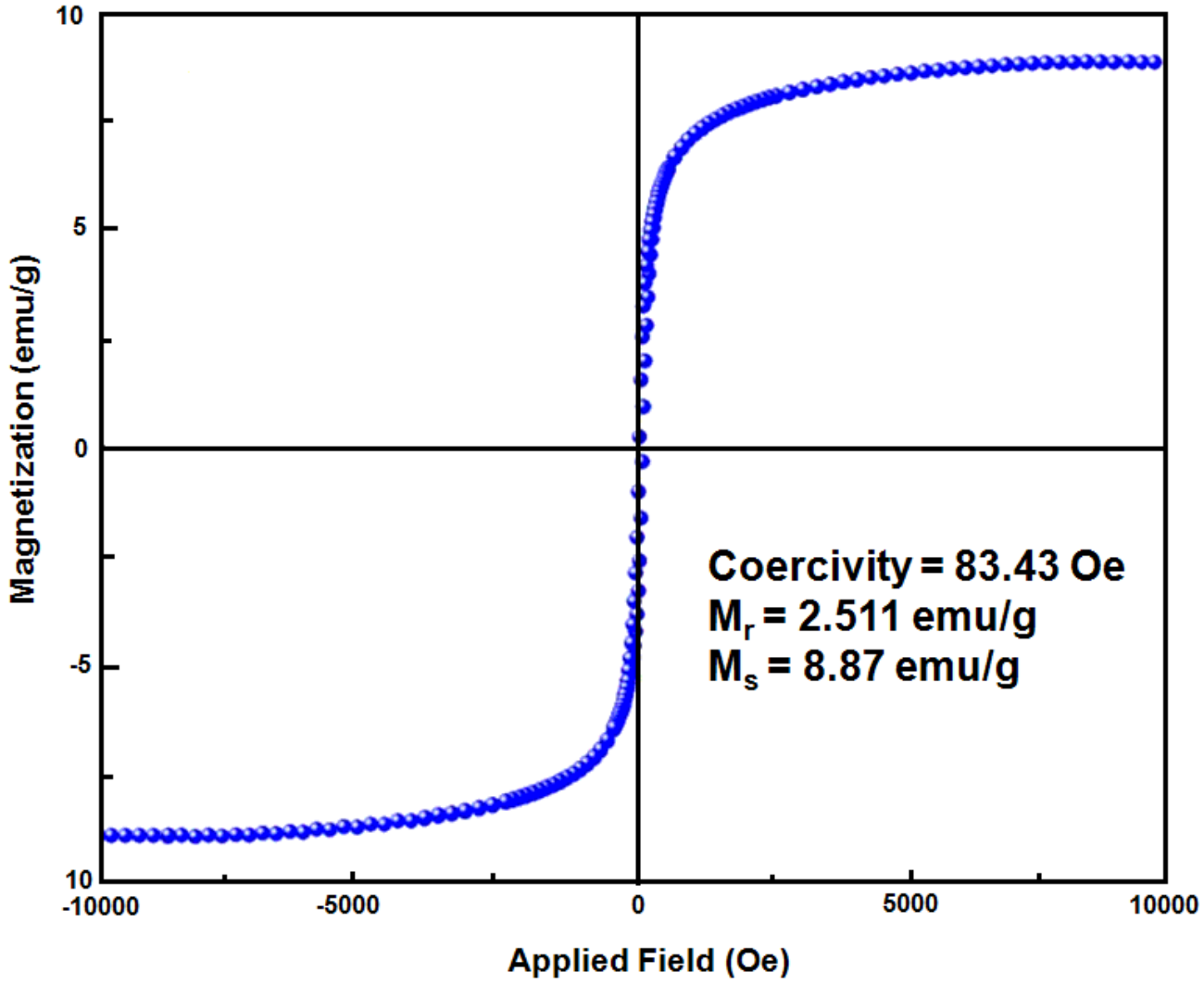

Figure 6

Hysteresis loop of prepared α-Fe2O3

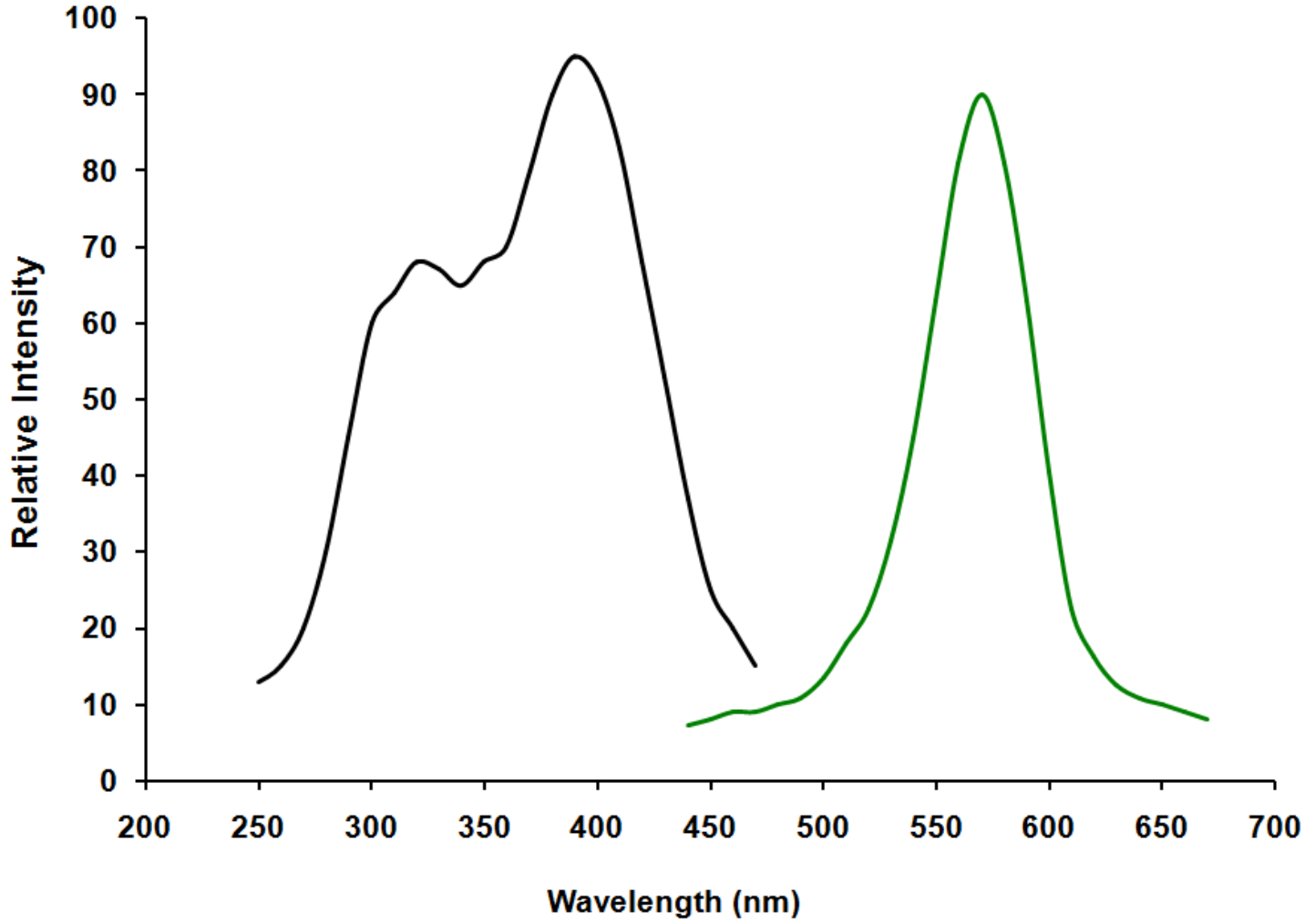

Figure 7

PL excitation and emission spectrum of α-Fe2O3

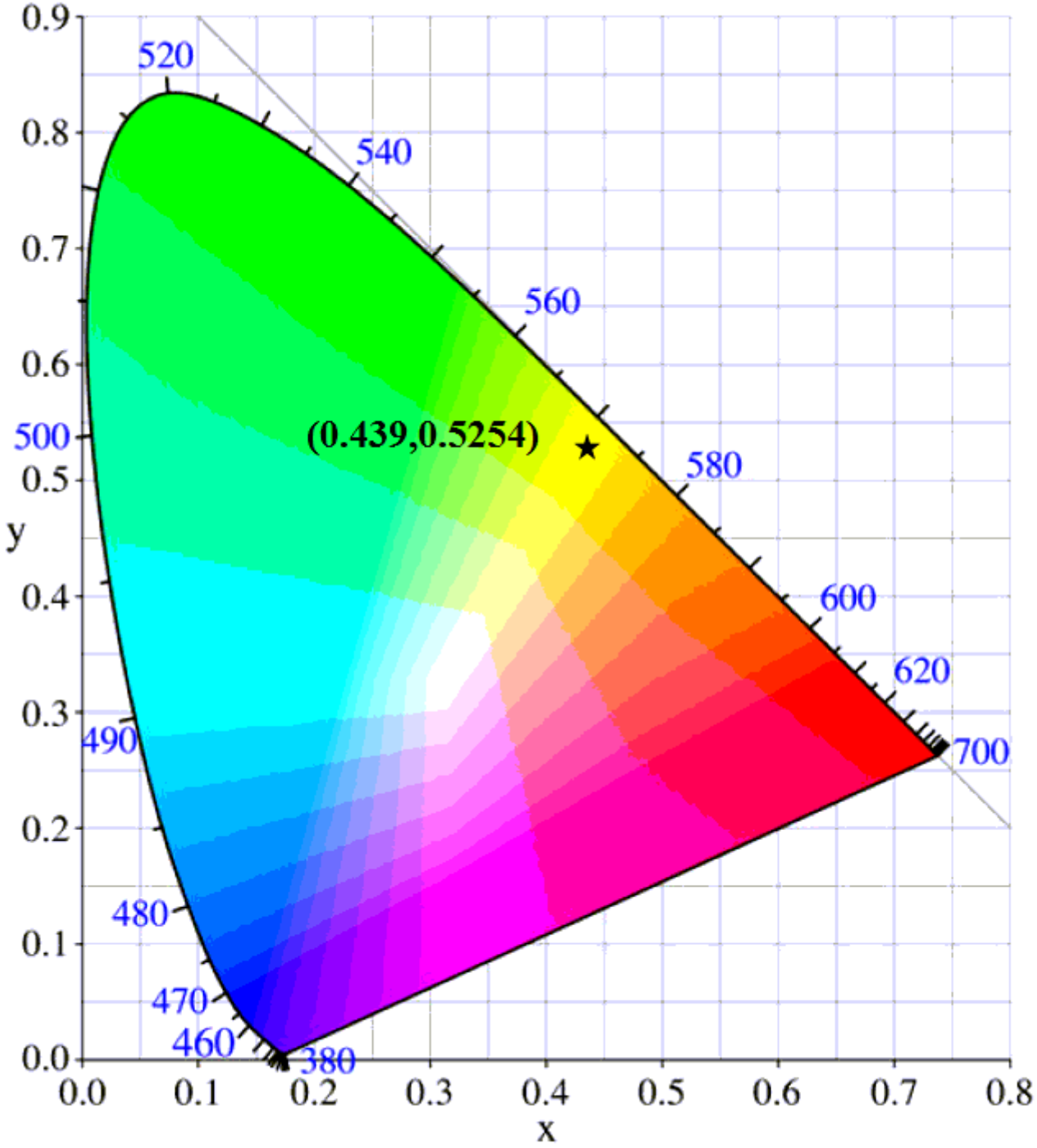

Figure 8

CIE chromaticity diagram

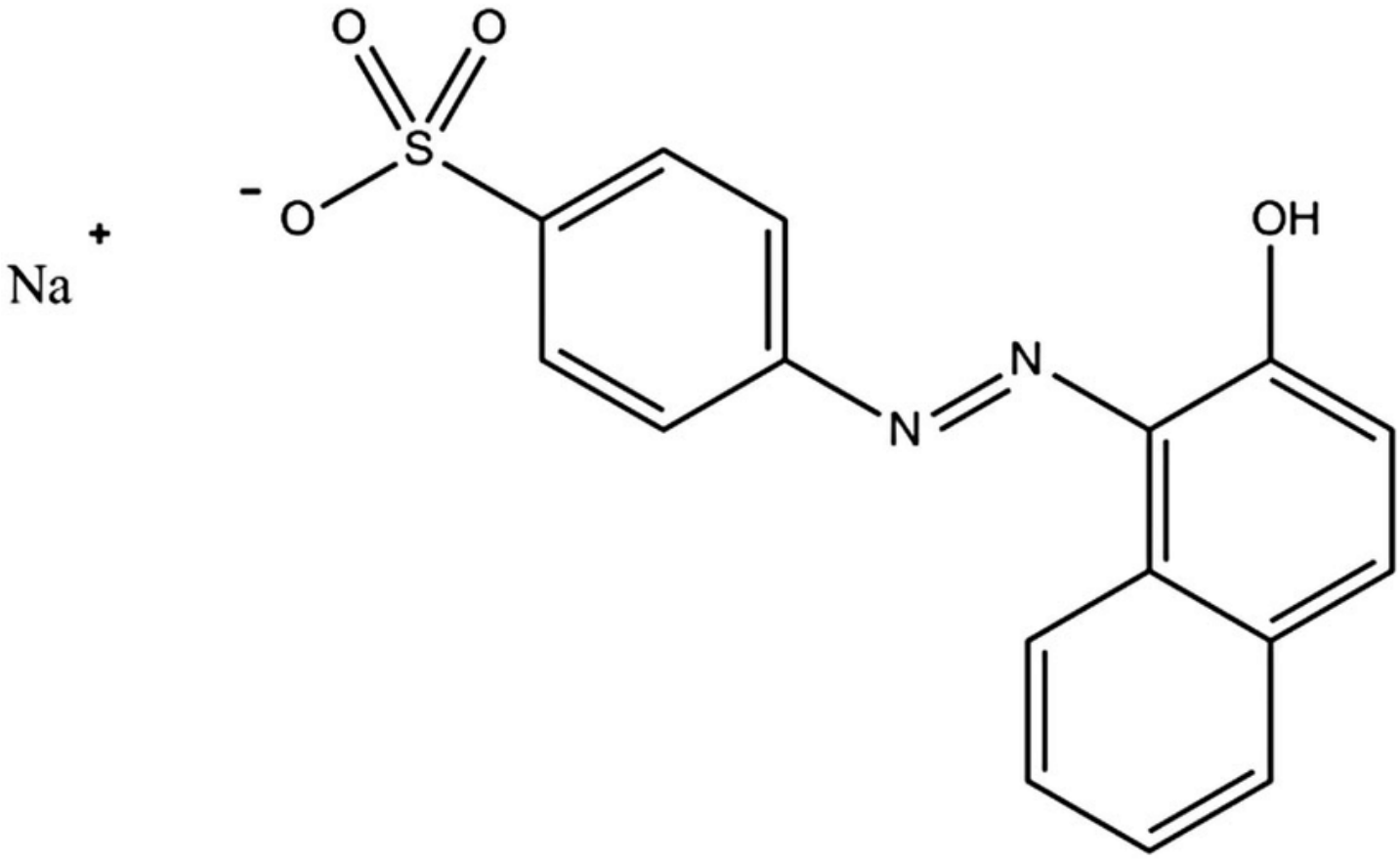

Figure 9

Structure of AO7

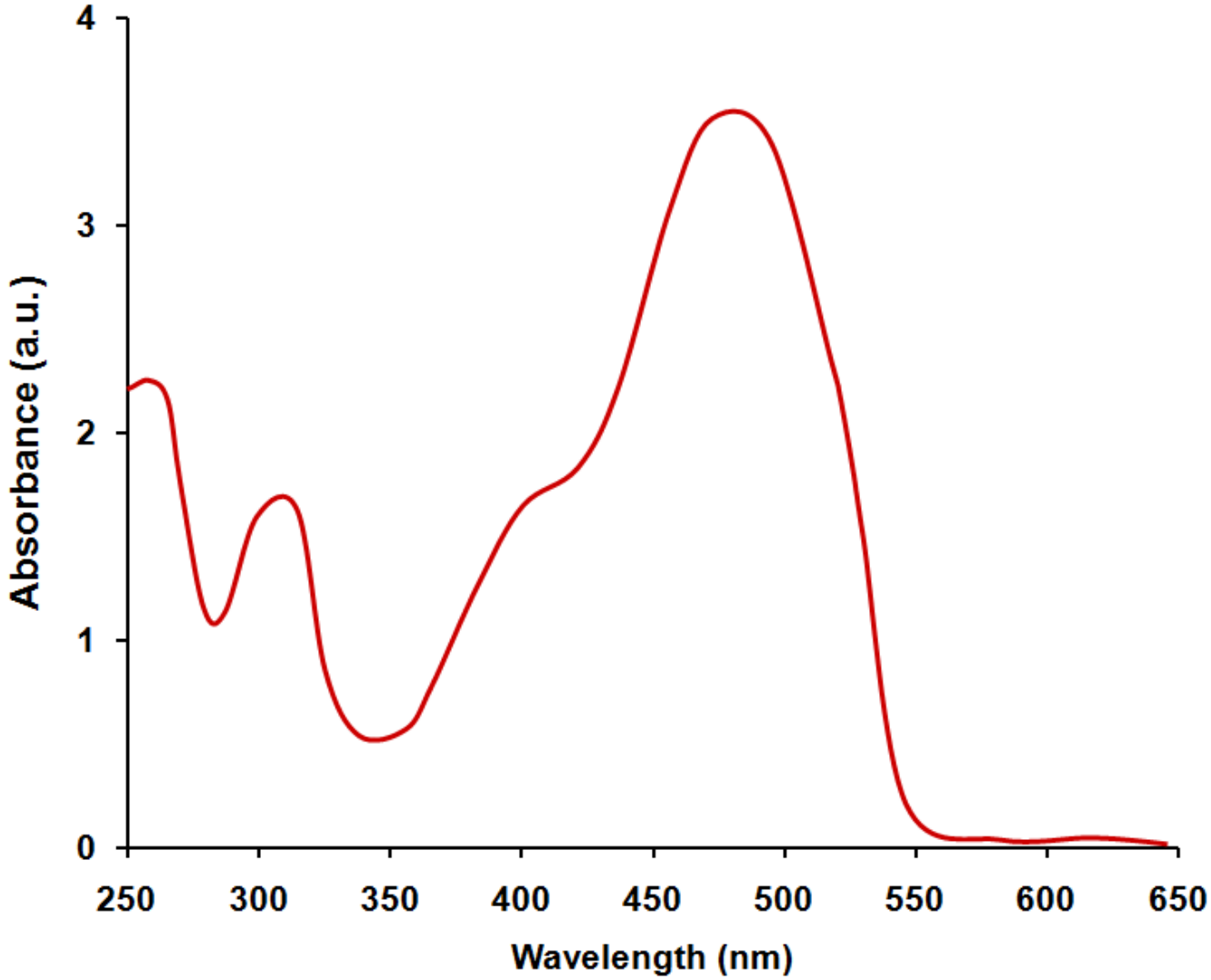

Figure 10

Absorption spectrum of AO7

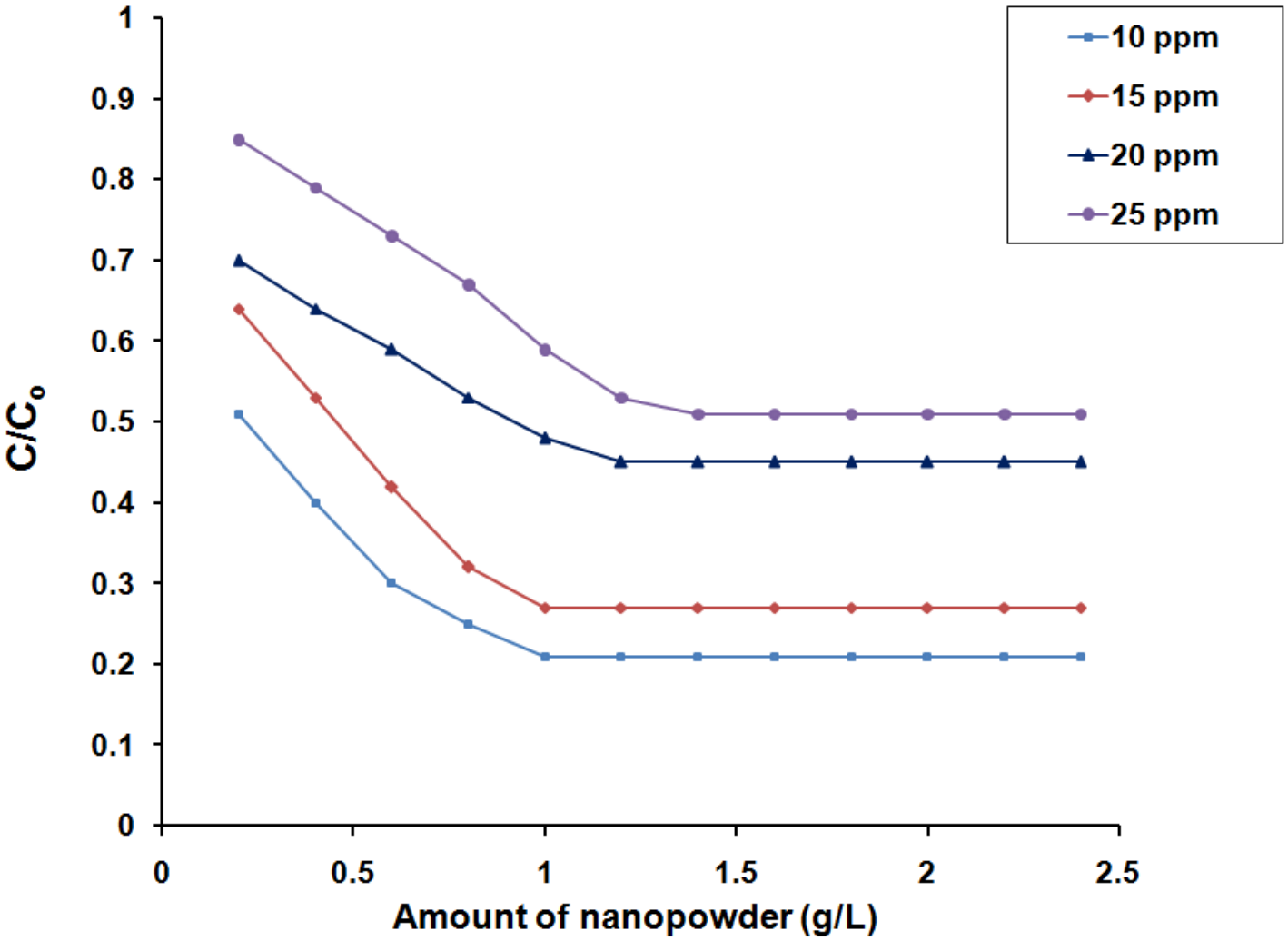

Figure 11

Effect of dosage of photocatalyst

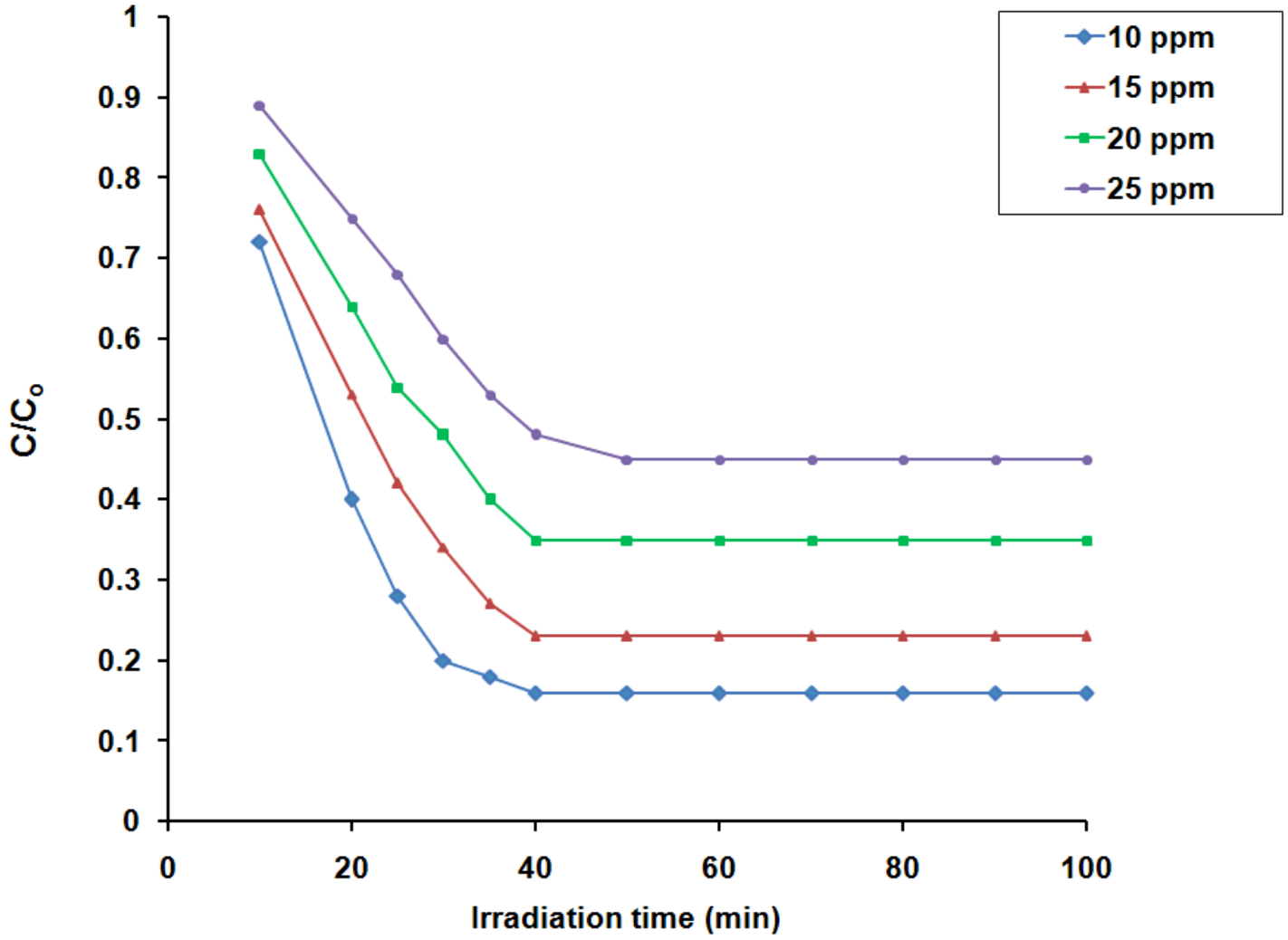

Figure 12

Effect of irradiation time